

A PHOTO-HADRONIC MODEL OF THE LARGE SCALE JETS OF 3C 273  
AND PKS 1136–135

MASAAKI KUSUNOSE<sup>1</sup> AND FUMIO TAKAHARA<sup>2</sup>

<sup>1</sup>*Department of Physics, Kwansei Gakuin University  
Gakuen 2-1, Sanda  
Hyogo, 669-1337, Japan*

<sup>2</sup>*Department of Earth and Space Science, Graduate School of Science, Osaka University  
Machikaneyama 1-1, Toyonaka, Osaka 560-0043, Japan*

Submitted to ApJ

ABSTRACT

X-ray bright knots of kpc-scale jets of several radio loud quasars have been an actively discussed issue. Among various models to explain observations, synchrotron radiation from the electron population different from radio to IR emitting electrons is promising. However, the origin of this electron population has been debated. Recently, we proposed that this electron population is produced by proton-photon collisions (mainly, Bethe-Heitler process), and we applied this model to PKS 0637–752. We found that this model works if the proton power is by an order of magnitude larger than the Eddington power. In this paper we apply this model to the X-ray emission in the knots of 3C 273 and PKS 1136–135. The target photons for electron-positron pair production are supplied by synchrotron radiation at radio-IR by primary electrons and by the active galactic nucleus (AGN) core as well as cosmic microwave background (CMB) radiation. The effects of the AGN photons are included for the first time in the hadronic model. Though the observed X-ray flux is obtained with the contribution of the AGN photons, the required proton power turns out to be highly super-Eddington. However, we find that our model works for a nearly Eddington proton power, if the photon density of the AGN is enhanced. This can occur if the AGN photons are more beamed toward the X-ray knots than toward our line of sight and the AGN photon frequency is shifted by the Doppler effect.

Corresponding author: Masaaki Kusunose  
[kusunose@kwansei.ac.jp](mailto:kusunose@kwansei.ac.jp), [takahara.fumio@wine.plala.or.jp](mailto:takahara.fumio@wine.plala.or.jp)

*Keywords:* quasars: general — quasars: individual (3C 273, PKS 1136–135) — galaxies: jets — X-rays: theory — radiation mechanisms: nonthermal

## 1. INTRODUCTION

Large scale jets of active galactic nuclei (AGNs) have been observed at various wavelengths. The kpc-scale jets of some AGNs are known to be bright in X-rays as observed with the *Chandra X-Ray Observatory* (Schwartz et al. 2000; Chartes et al. 2000). While the X-rays from FRI sources are usually explained by the extrapolation of the synchrotron spectrum at radio-IR emission, the X-ray flux of some quasars is larger than the flux extrapolated from the radio-IR radiation. Then various X-ray emission mechanisms for the kpc-scale jets have been proposed. Synchrotron-self Compton scattering by nonthermal electrons, which is often accepted as X-ray emission model for AGN jets, is not favored, because the required magnetic field is much weaker than the equipartition value (Chartes et al. 2000; Kataoka & Stawarz 2005). Inverse Compton (IC) scattering of cosmic microwave background (CMB) radiation in relativistically moving emission region beamed to the observer (IC/CMB model) was also considered (Tavecchio et al. 2000; Celotti et al. 2001). However, the predicted flux by IC/CMB model exceeds the upper limits of the  $\gamma$ -ray flux of kpc jets in PKS 0637–752 and 3C 273 observed by *Fermi* (Meyer & Georganopoulos 2014; Meyer et al. 2015). Additional  $\gamma$ -ray upper limits were recently presented for PKS 1136–135, PKS 1229–021, PKS 1354+195, and PKS 2209+080 (Breiding et al. 2017). Proton synchrotron model was also proposed (Aharonian 2002; Bhattacharyya & Gupta 2016), which requires a rather large value of magnetic fields, e.g., 10 mG.<sup>1</sup> The most promising model is synchrotron radiation by two different populations of electrons/positrons (Uchiyama et al. 2006), though different acceleration mechanisms for different electron/positron populations are to be considered. Liu et al. (2015) proposed shock regions in the knots of 3C 273: Different electron populations are formed in the upstream and the downstream, which correspond to radio-IR and X-ray emissions, respectively. Liu et al. (2017) recently proposed shear acceleration as a higher energy electron production mechanism. Though these are interesting possibilities and feasible energetically, detailed comparison between model prediction and observations is awaited.

Recently, to account for the second population of electrons, we proposed an alternative model in which high energy electrons/positrons produced by Bethe-Heitler process and applied this model to PKS 0637–752 (Kusunose & Takahara 2017). Protons obeying a power-law spectrum produce electrons/positrons (hereafter we call shortly electrons) in collisions with radio-IR photons emitted by synchrotron radiation in a knot. Then produced electrons emit X-rays and  $\gamma$ -rays by synchrotron radiation. We showed that X-ray emission is explained by this model with a size  $\sim$  a few kpc and a magnetic field  $\sim$  0.1 mG. However, the proton power an order of magnitude larger than the Eddington limit is required because of the low efficiency of electron produc-

<sup>1</sup> Aharonian (2002) first examined the various processes involving ultra high energy protons. He disfavored photo-hadronic processes because required proton power is too large. Instead he proposed proton synchrotron as reasonable but he assumed that protons escape the emission region diffusively. Considering a large proton pressure, protons will be adiabatically cooled. Thus, energy requirement is not relieved.

tion in the radiation field given by the radio-IR spectrum by primary electrons. It is to be noted that though the conversion efficiency of photo-pion production processes is larger, required proton energy is much larger and the produced electrons emit synchrotron photons at much higher energies than X-ray, which makes photo-pion processes relatively ineffective.

There are more AGNs with kpc-scale jets bright in X-rays and they can be used to examine our model. 3C 273 is one of these sources, a well known quasar at redshift  $z = 0.158$  (see Uchiyama et al. 2006, for review). Compared to PKS 0637–752, the luminosity of 3C 273 jet is lower and the slope between optical and X-rays is softer. However, the slope in the  $\log \nu$ - $\log \nu F_\nu$  representation at  $\sim 10^{15}$  Hz is still positive. Because of the  $\gamma$ -ray upper limits set by *Fermi* (Meyer et al. 2015) and the spectral shape of IR-optical through X-rays as well as the optical polarization (Uchiyama et al. 2006), the model with two electron populations is favored for 3C 273. Regarding the size of the emission region of kpc-scale knots, Marchenko et al. (2017) recently analyzed the detailed structure of the jet in 3C 273, and the knots were resolved to have extended features with the transverse sizes of  $\sim 0.5$  kpc and lengths  $\gtrsim 1$  kpc in X-rays and far-ultraviolet. This small size of the X-ray emission region is notable and it is worth studying the X-ray emission model by taking into account this small size, though this may be regarded as tentative because the results depend on a sophisticated deconvolution technique. The required proton power decreases with the decreasing size, when the target photon is provided internally. Another notable feature of 3C273 jet is different brightness distribution between X-rays and radio. While radio emission is brighter at the outer edge of the jet, X-rays are stronger at inner portion. This may suggest photons from the AGN core play some role in shaping the X-ray emission from the large scale jet. If the energy density of these photons in the knots dominates others, IC scattering by relativistic electrons and photo-hadronic processes are enhanced, which may somewhat relieve the energy problem. This effect is worth studying, because this has not been considered in previous work. Furthermore, photons from the AGN core are strongly beamed and the beamed direction is not necessarily peaked to the our line of sight. If the beaming is peaked toward the knots rather than our line of sight, the effects are much stronger.

Another kpc-scale jet is found in PKS 1136–135, a steep-spectrum quasar located at  $z = 0.556$ . The X-ray emitting knots of PKS 1136–135 are at projected distances of 30 - 60 kpc from the core (Cara et al. 2013). Sambruna et al. (2006) and Tavecchio et al. (2006) supported the IC/CMB model for the X-ray emission from the knots. On the other hand, Uchiyama et al. (2007) extensively studied the emission mechanisms in this source and interpreted the X-ray emission as synchrotron radiation from a second nonthermal electron population. Later Cara et al. (2013) found that several kpc-scale knots of PKS 1136–135 are highly polarized at optical. Combining this high polarization and the spectral shape, they concluded that IC/CMB models are not favored to explain the X-ray emission.

In this paper, we apply our model to the kpc-scale jets of 3C 273 and PKS 1136–135. In particular, we study the effect of AGN photons on the electron/positron production and consider its effect on the size of the emission region. In Section 2 we describe our model, and in Section 3 numerical results are shown. In Section 4 summary and discussion are presented. Throughout this paper we assume  $\Omega_m = 0.27$ ,  $\Omega_\Lambda = 0.73$ ,  $\Omega_r = 0$ , and  $H_0 = 71 \text{ km s}^{-1} \text{ Mpc}^{-1}$  for cosmological parameters.

## 2. ASSUMPTIONS AND FORMALISM

The model in this paper is the same as used in [Kusunose & Takahara \(2017\)](#) except that additional soft photon sources such as the AGN and CMB are considered. We also include proton synchrotron radiation as well as electron/positron production by photo-pion processes. However, for simplicity we do not include  $\gamma$ -ray production via  $\pi^0$  decay and subsequent cascade processes. We assume a uniform sphere with radius  $R$  for a knot with magnetic fields  $B$ . The relativistic bulk motion of the knot is not considered, because there is no clear evidence for relativistic motion of kpc-scale jets in 3C 273 and PKS 1136–135 (e.g., [Cara et al. 2013](#)), noting that only mildly relativistic beaming is enough to explain the asymmetry between the jet and the counter-jet. Radiation in radio through IR is emitted by nonthermal electrons in the knot. These electrons are the primary particles different from the secondary electrons produced by Bethe-Heitler process. The spectrum of these electrons is obtained by calculating the steady state solution of the kinetic equation of electrons with injection, radiative cooling, and escape. The kinetic equation for the primary electrons is given by

$$\frac{dn_e(\gamma_e)}{dt} = q_{\text{inj}}(\gamma_e) - \frac{n_e(\gamma_e)}{t_{\text{esc}}} - \frac{d}{d\gamma_e}[\dot{\gamma}_e n_e(\gamma_e)], \quad (1)$$

where  $\gamma_e$  is the electron Lorentz factor and  $n_e(\gamma_e)$  is the electron number density per unit interval of  $\gamma_e$ . Radiative processes are synchrotron radiation and IC scattering, and the cooling rate is denoted by  $\dot{\gamma}_e$ . The escape time of electrons,  $t_{\text{esc}}$ , is assumed to be  $3R/c$ , where  $c$  is the speed of light. To calculate the spectrum of the primary electrons that emit radio to IR, the injection spectrum of electrons is given by

$$q_{\text{inj}}(\gamma_e) = Q_e \gamma_e^{-\alpha_e} H(\gamma_e - \gamma_{e,\text{min}}) H(\gamma_{e,\text{max}} - \gamma_e), \quad (2)$$

where  $H(x)$  is the Heaviside function defined as  $H(x) = 1$  for  $x > 0$  and  $H(x) = 0$  for  $x < 0$ . Here we do not specify the acceleration mechanisms to produce the injection spectrum.

In the same knot, nonthermal protons produce electrons via collisions with soft photons. The protons obey a power law given by

$$n_p(\gamma_p) = K_p \gamma_p^{-\alpha_p} H(\gamma_p - \gamma_{p,\text{min}}) H(\gamma_{p,\text{max}} - \gamma_p), \quad (3)$$

where  $\gamma_p$  is the proton Lorentz factor and  $n_p(\gamma_p)$  is the proton number density per unit interval of  $\gamma_p$ . We do not solve the kinetic equation for protons, because

**Table 1.** Parameters for the primary electrons with  $f_A = 1$ 

	$R$ (kpc)	$B$ (mG)	$\alpha_e$	$\gamma_{e,\min}$	$\gamma_{e,\max}$
3C 273 knot A & B1	5	0.1	1.9	10	$7 \times 10^5$
3C 273 knot A & B1	0.5	0.1	2.4	10	$9 \times 10^5$
1136–135 knot A	5	0.1	2.1	10	$10^6$
1136–135 knot B	5	0.1	1.9	10	$9 \times 10^5$

the cooling time of protons is much longer than that of electrons. Then the production spectrum of electrons is calculated for a given proton spectrum according to Kelner & Aharonian (2008). To calculate the second population of electrons that emit the X-rays,  $q_{\text{inj}}(\gamma_e)$  in Equation (1) is replaced by the electron/positron production spectrum by Bethe-Heitler process and photo-pion processes based on Kelner & Aharonian (2008). The soft photons used in electron production are supplied by radio-IR emission via above mentioned synchrotron radiation by the primary electrons. In addition to these soft photons emitted in the knot, radiation from the AGN and CMB is included. The distance of the knot from the AGN core is denoted by  $d_{\text{knot}}$ . To calculate the soft photon injection rate from the AGN, we use the photon spectrum compiled by NED. Though the dispersion is large in the photon spectrum, we use a polynomial fit in  $\log \nu$ - $\log F_\nu$  plot of the NED spectrum. As was mentioned in §1, the beamed direction of AGN photons is not necessarily peaked to our line of sight and knots may receive a larger flux than that observed by us. When we introduce the enhancement of the AGN photons due to this effect, we use a parameter  $f_A$  to denote the enhancement factor of the AGN photon number flux per unit frequency. We also consider the frequency shift of AGN photons by the Doppler effect  $f_A^{1/2}$ . The effect of CMB photons on electron production is not important in our model, because the relativistic bulk motion of the knot is not considered. The produced electrons emit photons by synchrotron radiation and IC scattering. Here the latter contribution to the X-rays is negligible. In this work proton synchrotron is also included. However, because the magnetic field is weak, e.g.,  $\sim 0.1$  mG, proton synchrotron has only minor effect on the emission spectrum.

Parameters for numerical calculations are  $R$ ,  $B$ ,  $d_{\text{knot}}$ ,  $f_A$ ,  $K_p$ ,  $\gamma_{p,\min}$ ,  $\gamma_{p,\max}$ ,  $\alpha_p$ ,  $Q_e$ ,  $\gamma_{e,\min}$ ,  $\gamma_{e,\max}$ , and  $\alpha_e$ . We set  $\gamma_{p,\min} = 1$  throughout the paper.

### 3. RESULTS

#### 3.1. 3C 273

The jet of 3C 273 has been frequently observed at various wavelengths (see Marchenko et al. 2017, for review). The  $\gamma$ -ray upper limits on the knots A and B1

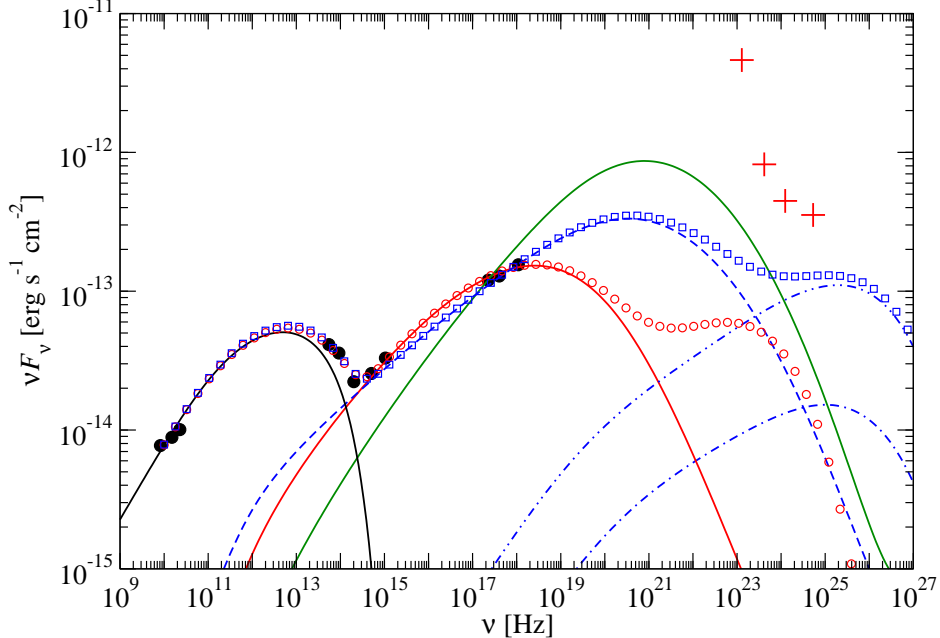


**Figure 1.** The spectral energy distribution of 3C 273 knots A and B1 combined (filled circles). Crosses are the upper limits set by *Fermi*. The models are produced for  $R = 5$  kpc and  $B = 0.1$  mG. The solid black line is synchrotron radiation by primary electrons (parameters are given in Table 1). The solid green line is synchrotron radiation by electrons/positrons by Bethe-Heitler process for  $\alpha_p = 2$ ,  $\gamma_{p,\max} = 10^{10}$ , and  $K_p = 6 \times 10^{-4} \text{ cm}^{-3}$  without AGN photons. The dashed blue line is for  $\alpha_p = 2.3$ ,  $\gamma_{p,\max} = 10^{10}$ , and  $K_p = 0.154 \text{ cm}^{-3}$  with AGN photons ( $f_A = 1$ ). For these parameters, synchrotron spectra by positrons and electrons from photo-pion processes are shown by dot-dot-dashed and dot-dashed blue lines, respectively. The total emission of these spectra is shown by blue open squares. Solid red line is for  $\alpha_p = 1.9$ ,  $\gamma_{p,\max} = 5 \times 10^8$ , and  $K_p = 1.77 \times 10^{-4} \text{ cm}^{-3}$  with AGN photons ( $f_A = 1$ ). The total emission for these parameters is shown by red open circles. The bump around  $10^{23}$  Hz is the contribution from synchrotron radiation by positrons from photo-pion processes.

observed by *Fermi* are shown in Meyer et al. (2015). Though previous observations did not set strong constraints on the size of the emission regions, Marchenko et al. (2017) recently resolved the X-ray emission region down to  $\sim 0.5$  kpc. Considering that their result needs further confirmation, in this work we make models for  $R = 5$  kpc and 0.5 kpc.

### 3.1.1. Models with $R = 5$ kpc

We first show our models for  $R = 5$  kpc and  $B = 0.1$  mG in Figure 1. The observed data are from Meyer et al. (2015). The emission spectrum is fitted to the spectrum of knots A and B1 combined. The parameters for primary electrons that emit radio-IR are given in Table 1. The injection spectrum is harder than the steady state electron spectrum because of radiative cooling. The X-ray spectrum strongly depends on  $\alpha_p$  and  $\gamma_{p,\max}$ . However, because the data for the X-rays are limited, we cannot uniquely determine the values of these parameters. In Figure 1, we show models with and without AGN photons. The solid green line is for a model without AGN photons,

where  $\alpha_p = 2$ ,  $\gamma_{p,\max} = 10^{10}$ , and  $\gamma_{p,\min} = 1$ . (In this model photo-pion processes are not taken into account.) When the photons from the AGN are not included, the synchrotron spectrum by electrons produced by Bethe-Heitler process is harder than the observed one at optical to X-rays. We find that this is true as long as  $\alpha_p \lesssim 2.7$  when  $\gamma_{p,\max} = 10^{10}$ . (Compared to PKS 0637–752, the observed spectrum of 3C 273 at optical to X-ray is softer.) Then for  $\alpha_p \lesssim 2.7$ , it is difficult to fit optical and X-rays simultaneously. On the other hand, when the value of  $\alpha_p$  is larger, energy requirement becomes larger.

When the AGN photons are included, the value of  $\alpha_p$  can be smaller. Here we assume  $d_{\text{knot}} = 50$  kpc to determine the photon flux from the AGN. Since the angle between the line of sight and the jet direction is not known, the value of  $d_{\text{knot}}$  in our models should be taken as a characteristic value. The spectra of target photons in electron production are shown in Figure 2. The AGN photon spectrum is based on the data from NED. For the most part we assume that knots receive the same flux of AGN photons as the observed one, though we take into account for the distances of knots from the AGN. In the following we assume  $f_A = 1$  and the effects of the beaming of AGN photons are discussed in §3.1.4. For  $d_{\text{knot}} = 50$  kpc, the photons from the AGN core dominate when  $R = 5$  kpc. We first fix the value of  $\gamma_{p,\max} = 10^{10}$  to calculate the electron production rate. We find that  $\alpha_p$  must be smaller than 2.4 to fit the data. When  $\alpha_p \gtrsim 2.4$  with a fixed value of  $\gamma_{p,\max} = 10^{10}$ , the electron spectrum becomes steeper and the number density of electrons with  $\gamma_e \sim 10^5$  becomes larger. As a result the flux at optical becomes too large. When  $\alpha_p = 2.3$ , for example,  $K_p = 0.15 \text{ cm}^{-3}$  explains the observed spectrum as depicted by the dashed blue line for Bethe-Heitler process in Figure 1. Radiation from positrons and electrons from photo-pion origin is shown by dot-dot-dashed and dot-dashed blue lines, respectively. Their contribution is mainly above 10 GeV and does not exceed the Fermi limits. The sum is shown by blue squares. When the value of  $\alpha_p$  is much smaller, the value of  $\gamma_{p,\max}$  should be smaller too to fit the data. When  $\alpha_p = 1.9$ , we find  $\gamma_{p,\max} = 5 \times 10^8$  with  $K_p = 1.8 \times 10^{-4} \text{ cm}^{-3}$  fit the data as depicted by the solid red line for Bethe-Heitler process in Figure 1. The sum of Bethe-Heitler and photo-pion processes is shown by red squares. This smaller value of  $\gamma_{p,\max}$  is chosen to suppress over-production of X-rays. The  $\gamma$ -ray flux in our model is well below the *Fermi* upper limits, as is the case for PKS 0637–752 (Kusunose & Takahara 2017). When  $\alpha_p \lesssim 1.8$ , the spectrum at optical-IR is too hard irrespective of the value of  $\gamma_{p,\max}$ .

The electron spectra for the models with  $R = 5$  kpc and AGN photons are shown in Figure 3. In the production spectrum of electrons,  $\gamma_e^2 n_e(\gamma_e)$  from Bethe-Heitler process has a peak at  $\gamma_e \sim 2 \times 10^8$  for  $\alpha_p = 1.9$  and  $\gamma_{p,\max} = 5 \times 10^8$ . Because of radiative cooling the peak is located at the lower energy,  $\gamma_e \sim 10^5$ , in the steady state. In the figure, the spectra of electrons and positrons by photo-pion processes are also shown.



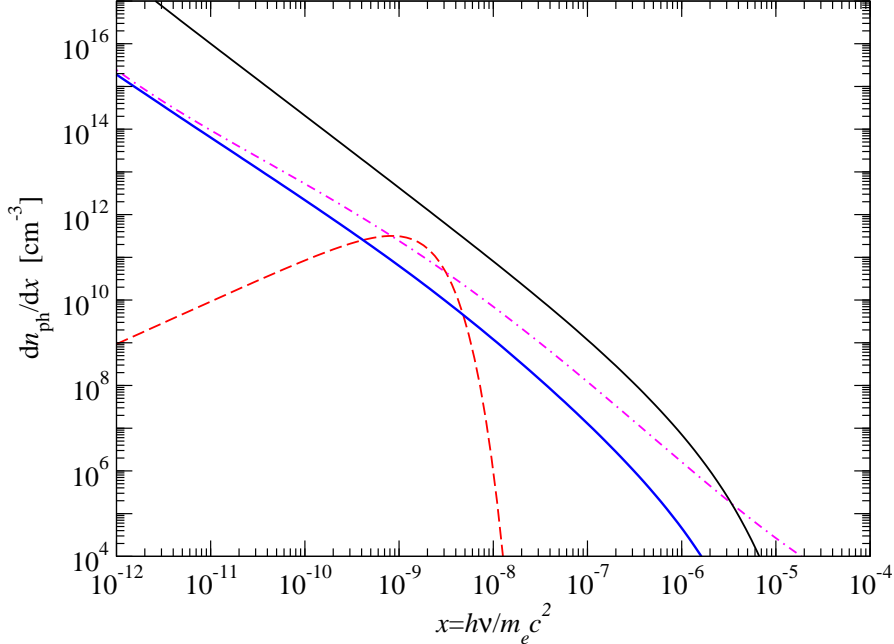


**Figure 2.** The target photon spectra in a knot of 3C 273. The black and blue solid lines are the radiation at radio-IR band emitted by the primary electrons in knots A and B1 combined for  $R = 0.5$  kpc and 5 kpc, respectively. The dashed line is the radiation field of CMB and the dot-dashed line is radiation emitted by the AGN core assuming  $d_{\text{knot}} = 50$  kpc.

As mentioned above, we used the NED data for the AGN spectrum. The NED data of the photon spectrum have a large dispersion. To examine the effect of the NED photon spectrum we artificially varied the photon spectrum from the AGN (Figure 4). The results are shown in Figure 5 for  $\alpha_p = 2.3$  and  $\gamma_{p,\text{max}} = 10^{10}$ . It is found that the X-ray spectrum does not strongly depend on the AGN spectrum.

### 3.1.2. Models with $R = 0.5$ kpc

According to Marchenko et al. (2017), the size of knot A is resolved down to  $\sim 0.5$  kpc for the X-ray emission region. We present models for  $R = 0.5$  kpc and  $B = 0.1$  mG in Figure 6, assuming that the spatial extent of radio-IR knots is 0.5 kpc as well. When  $R = 0.5$  kpc and  $d_{\text{knot}} = 50$  kpc, photons from the AGN core are not important as long as  $f_A = 1$  and CMB photons have only minor effects (Fig. 2). The injection spectrum of the primary electrons is softer ( $\alpha_e = 2.4$ ) than that for the models with  $R = 5$  kpc. In Figure 6, we show a model with  $\alpha_p = 1.9$ ,  $\gamma_{p,\text{max}} = 5 \times 10^8$ , and  $K_p = 1.68 \times 10^{-2} \text{ cm}^{-3}$ . Compared to the model with  $R = 5$  kpc, the value of  $K_p$  is increased by  $10^2$ . As  $R$  decreases the contribution of the radiation from the AGN decreases while the radio-IR photon density in a knot increases. We also calculated a model with  $\alpha_p = 2.3$  and  $\gamma_{p,\text{max}} = 10^{10}$  as for  $R = 5$  kpc and find that  $K_p = 18 \text{ cm}^{-3}$  fits the observed X-rays.

### 3.1.3. Proton power

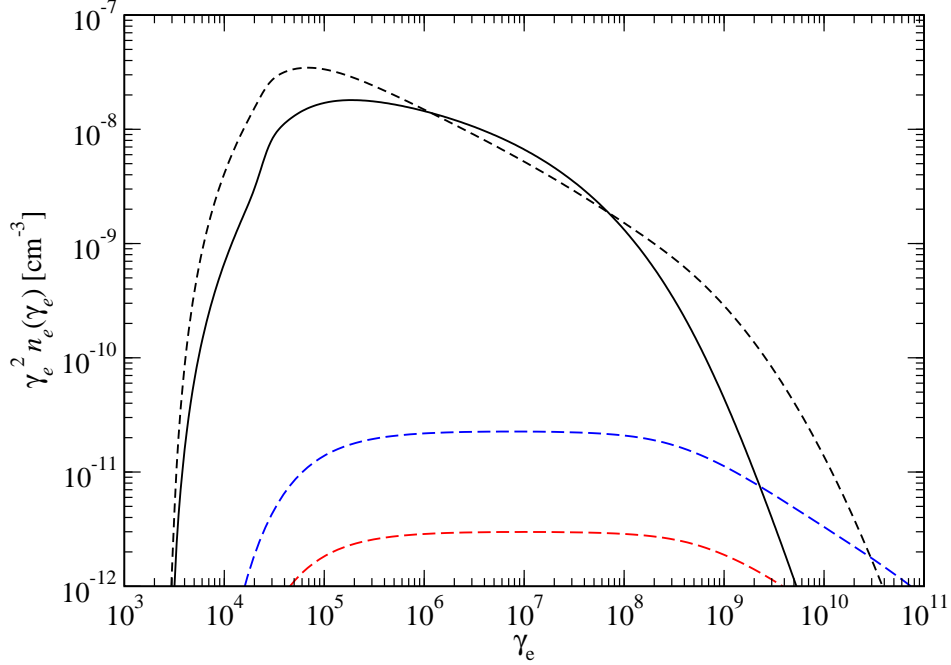


**Figure 3.** The steady state spectra of electrons produced by hadronic processes in a knot of 3C 273 with  $f_A = 1$ . Electron/positron spectra produced by Bethe-Heitler process are shown by the solid line for  $\alpha_p = 1.9$  and  $\gamma_{p,\max} = 5 \times 10^8$  and the dashed line for  $\alpha_p = 2.3$  and  $\gamma_{p,\max} = 10^{10}$ . The spectra of positrons and electrons via photo-pion processes are shown by the blue and red dashed lines, respectively, for the model with  $\alpha_p = 2.3$  and  $\gamma_{p,\max} = 10^{10}$ .

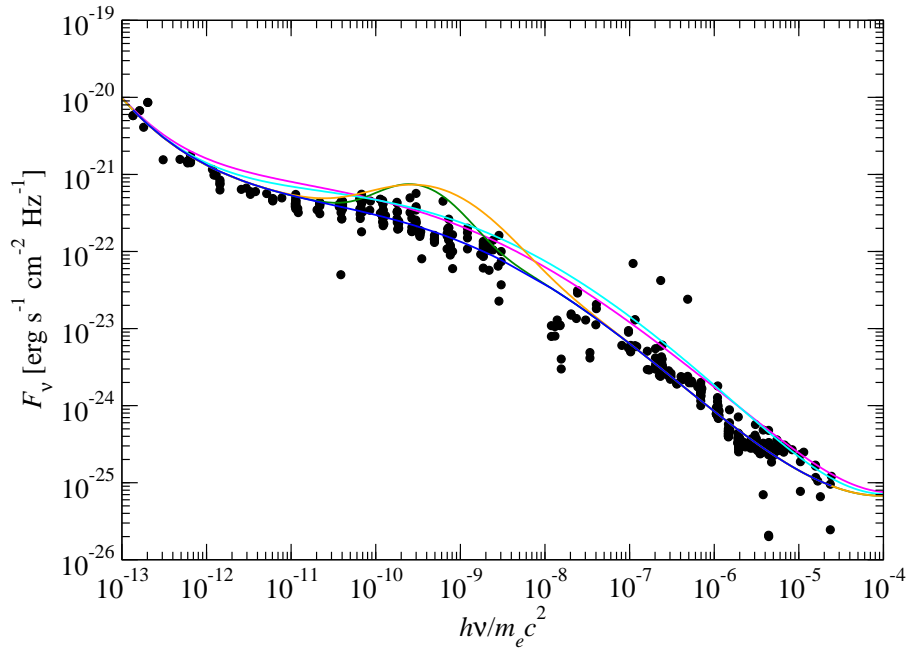


**Figure 4.** The radiation spectrum of 3C 273. Filled circles are the data from NED. The blue line is used to construct our models. Other various lines are used in Figure 5.

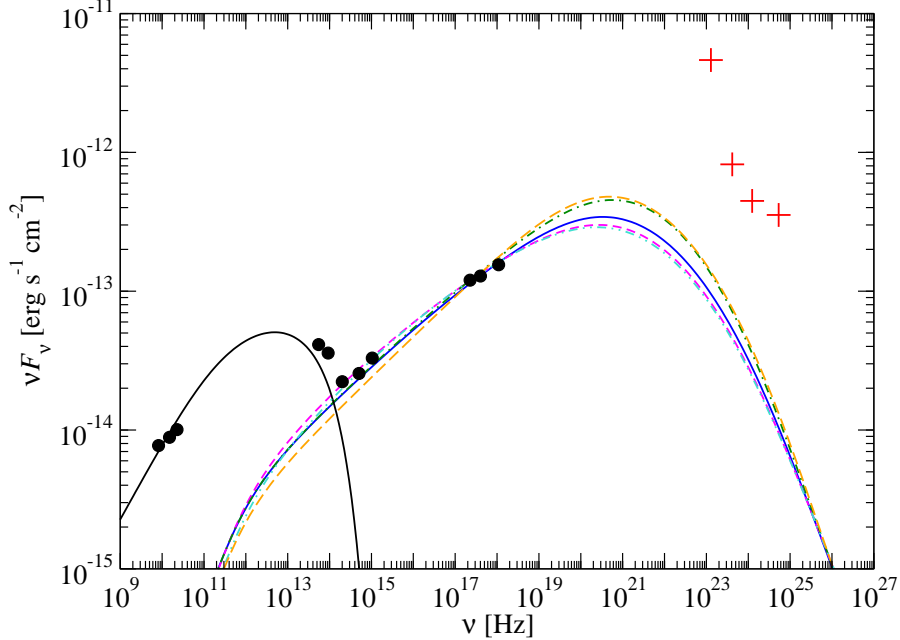


**Figure 5.** The spectral energy distribution of knots A and B1 combined of 3C 273 for various target photon spectra supplied by the AGN with  $f_A = 1$  (Fig. 4). Here  $\alpha_p = 2.3$  and  $\gamma_{p,\max} = 10^{10}$ ,  $R = 5$  kpc,  $B = 0.1$  mG, and  $d_{\text{knot}} = 50$  kpc. The blue line is the same as shown in Figure 1 for  $\alpha_p = 2.3$ . Other colors of lines correspond to the same colors shown in Figure 4. For simplicity, photo-pion processes are not shown.

The proton energy,  $U_p$ , in a knot is calculated for our models with  $f_A = 1$ . For  $\alpha_p = 2.3$ ,  $K_p = 0.15 \text{ cm}^{-3}$ ,  $\gamma_{p,\max} = 10^{10}$ , and  $R = 5$  kpc, we obtain  $U_p \sim 1.2 \times 10^{64}$  erg. For  $\alpha_p = 1.9$ ,  $K_p = 1.8 \times 10^{-4} \text{ cm}^{-3}$ ,  $\gamma_{p,\max} = 5 \times 10^8$ , and  $R = 5$  kpc, the proton energy is  $\sim 2.6 \times 10^{62}$  erg. If the proton power is estimated as  $L_p \sim U_p / (3R/c)$ , where  $3R/c$  is the escape time (or adiabatic cooling time) of protons, these models result in  $L_p \gtrsim 10^{50} \text{ erg s}^{-1}$ . The black hole mass  $M_{\text{BH}}$  of 3C 273 is estimated to be  $\sim 10^8 M_\odot$  (Espaillat et al. 2008, and references therein), while Paltani & Türler (2005) estimate  $M_{\text{BH}} \sim 7 \times 10^9 M_\odot$ . It is found that  $L_p \sim 10^2 - 10^4 L_{\text{Edd}}$  for  $M_{\text{BH}} = 10^{10} - 10^8 M_\odot$ ,  $\alpha_p = 1.9$ ,  $K_p = 1.8 \times 10^{-4} \text{ cm}^{-3}$ , and  $\gamma_{p,\max} = 5 \times 10^8$ . Here  $L_{\text{Edd}} \sim 1.26 \times 10^{47} (M/10^9 M_\odot) \text{ erg s}^{-1}$  is the Eddington luminosity. When  $R = 0.5$  kpc,  $U_p = 2.5 \times 10^{61}$  erg and  $L_p \sim 1.6 \times 10^{50} \text{ erg s}^{-1} \sim 10^3 L_{\text{Edd}}$  for  $M_{\text{BH}} = 10^9 M_\odot$ ,  $\alpha_p = 1.9$ ,  $\gamma_{p,\max} = 5 \times 10^8$ , and  $K_p = 1.7 \times 10^{-2} \text{ cm}^{-3}$ .  $L_p$  does not much depend on the value of  $R$  and  $K_p$  is nearly proportional to  $R^{-2}$  when  $\alpha_p$  is fixed. The details of the energy density,  $u_p$ , and power of protons as well as the energy density of the primary electrons,  $u_e$ , are shown in Table 2. These models need the proton power larger than the Eddington luminosity by a few orders of magnitude and are hard to realize.

#### 3.1.4. Beaming of AGN photons

The required large proton power may be eased if the following situation is realized. Though the AGN core of 3C 273 is known to exhibit super luminal motion, the beam

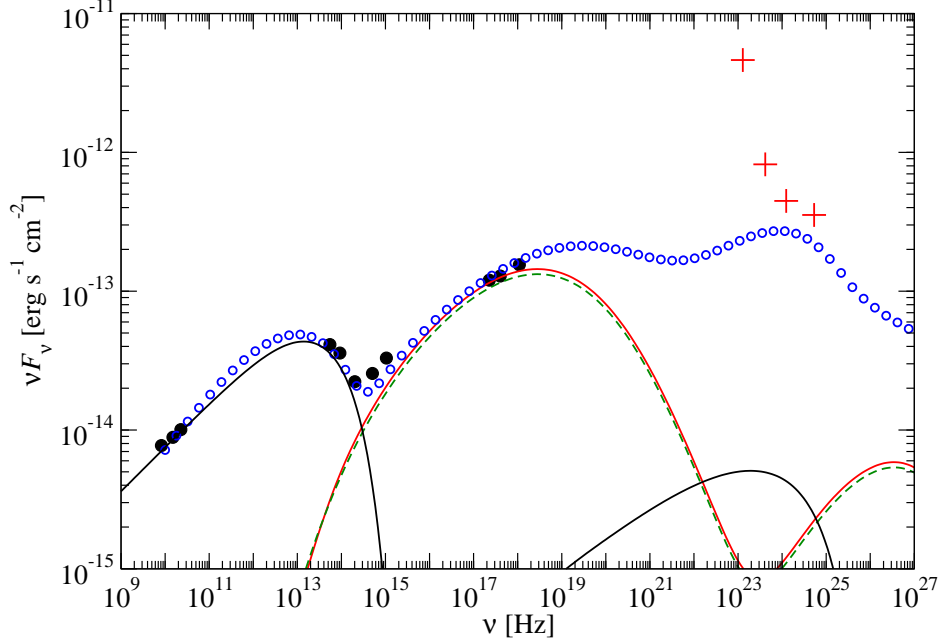


**Figure 6.** Models of 3C 273 for  $R = 0.5$  kpc and  $B = 0.1$  mG. Black solid line: Synchrotron and synchrotron self-Compton emission by the primary electrons. Radiation by electrons/positrons produced by Bethe-Heitler process is calculated for  $\alpha_p = 1.9$  and  $\gamma_{p,\max} = 5 \times 10^8$ . Red solid line:  $f_A = 1$ ,  $K_p = 1.68 \times 10^{-2} \text{ cm}^{-3}$ , and  $d_{\text{knot}} = 50$  kpc. Green dashed line: Without AGN photons, and other parameters are the same as those for the red solid line. With AGN photons and  $f_A = 40$ , the sum of emission by the primary electrons and electrons/positrons by Bethe-Heitler and photo-pion processes are shown by open circles, where  $\alpha_p = 1.98$ ,  $\gamma_{p,\max} = 2 \times 10^9$ , and  $K_p = 5.5 \times 10^{-4} \text{ cm}^{-3}$ .

direction of radiation from the core can be slightly off the line of sight and is towards the kpc-scale jets. Then we observe a smaller flux of the AGN radiation and the knots receive the enhanced flux by the relativistic beaming effect. In the following we assume that a knot receives the AGN photon number flux per unit frequency enhanced by  $f_A$  compared with the flux that we receive and the frequency is shifted by  $f_A^{1/2}$  in the knot frame. To reduce the required large power of protons to as small as  $10^{47} \text{ erg s}^{-1}$ , the Doppler factor of the AGN core about a few times larger than we observe is necessary. Note that the radiation spectrum of 3C 273 core is not like a typical blazar, which is consistent with this hypothesis. Here we remark that when there are enhanced AGN photons, IC scattering off the AGN photons by the primary electrons is also enhanced.

Results for  $f_A = 1, 10, 20, 40$ , and  $80$  with  $R = 5$  kpc and  $B = 0.1$  mG are shown in Figure 7. The values of  $\alpha_p$  and  $\gamma_{p,\max}$  are given in Table 3. The injection spectrum of the primary electrons are varied according to the value of  $f_A$ . As the value of  $f_A$  becomes larger, a harder injection spectrum is applied because radiative cooling becomes more effective by IC scattering off AGN photons. The contribution of IC scattering off AGN photons by primary electrons is shown in Figure 7 for  $f_A = 40$ . The peak of IC scattering appears in the GeV region. Synchrotron emission by

electrons/positrons via photo-pion processes is also shown for  $f_A = 40$ . For various values of  $R$  and  $f_A$ , the energy density and power of protons are given in Table 3. The upper limit of the value of  $f_A$  is set by IC scattering by primary electrons and synchrotron radiation of positrons. When  $f_A \lesssim 80$ , synchrotron emission by Bethe-Heitler electrons can explain the X-rays without violating the *Fermi* limits. The necessary proton power can be as small as  $L_{\text{Edd}}$  for large enough values of  $f_A$ . The visual luminosity of 3C 273 is  $\sim 10^{46}$  erg s $^{-1}$  (Fan et al. 2009). If  $f_A = 10$ -40, the enhanced luminosity becomes  $\sim 10^{48}$ - $10^{49}$  erg s $^{-1}$  and is near the most luminous blazar (e.g. Ghisellini et al. 2017). When  $R = 0.5$  kpc, the effect of AGN photons is weak if  $f_A = 1$  as shown in Figure 2. However, if  $f_A \gtrsim 10$ , the AGN photons are effective to reduce the proton power. These effects of the AGN photons are shown in Figure 6 for  $f_A = 40$ .

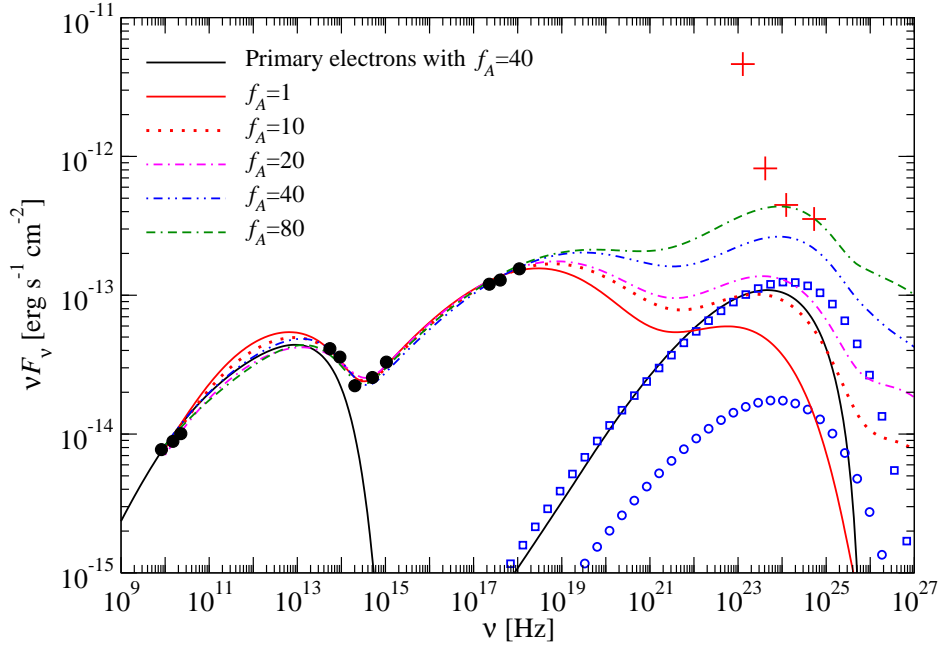


**Figure 7.** Models of 3C 273 for  $R = 5$  kpc and  $B = 0.1$  mG with  $f_A = 1, 10, 20, 40,$  and  $80$ . The spectra are the sum of IC scattering off AGN photons by primary electrons and synchrotron radiation by primary electrons and electrons/positrons produced by Bethe-Heitler and photo-pion processes. Note that for  $f_A = 1$ , there is no contribution from IC scattering by primary electrons. The values of  $\alpha_p$  and  $\gamma_{p,\text{max}}$  are given in Table 3. For  $f_A = 40$ , emission by primary electrons is shown by a solid black line and the spectra by positrons and electrons via photo-pion processes are shown by open squares and circles, respectively. There is a significant contribution of IC scattering off AGN photons by primary electrons for  $f_A \gtrsim 20$ .

### 3.1.5. Summary of 3C 273

In this subsection we have presented a hadronic model to explain the X-ray emission from the kpc-scale jet in 3C 273. The X-rays are produced by synchrotron radiation emitted by electrons produced by Bethe-Heitler process. The target photons are

**Table 2.** Proton energy density and power of 3C 273 for  $f_A = 1$ 

$R$ (kpc)	$u_e$ (erg cm <sup>-3</sup> )	$\alpha_p$	$\gamma_{p,\max}$	$u_p$ (erg cm <sup>-3</sup> )	$L_p$ (10 <sup>50</sup> erg s <sup>-1</sup> )
0.5	$4.6 \times 10^{-8}$	1.9	$5 \times 10^8$	$1.6 \times 10^{-3}$	1.6
1	$4.9 \times 10^{-9}$	1.9	$5 \times 10^8$	$6.6 \times 10^{-4}$	2.6
1	$4.9 \times 10^{-9}$	2.3	$10^{10}$	$3.3 \times 10^{-2}$	$1.3 \times 10^2$
5	$1.3 \times 10^{-11}$	1.9	$5 \times 10^8$	$1.7 \times 10^{-5}$	1.7
5	$1.3 \times 10^{-11}$	2.3	$10^{10}$	$7.7 \times 10^{-4}$	$7.7 \times 10$

NOTE—The magnetic energy density is  $u_{\text{mag}} = 4.0 \times 10^{-10}$  erg cm<sup>-3</sup> for  $B = 0.1$  mG.

**Table 3.** Proton energy density and power of 3C 273 for various values of  $R$  and  $f_A$ 

$R$ (kpc)	$f_A$	$\alpha_p$	$\gamma_{p,\max}$	$u_p$ (erg cm <sup>-3</sup> )	$L_p$ (erg s <sup>-1</sup> )
0.5	10	1.98	$9 \times 10^8$	$3.1 \times 10^{-4}$	$3.1 \times 10^{49}$
0.5	20	1.95	$10^9$	$7.1 \times 10^{-5}$	$7.1 \times 10^{48}$
0.5	40	1.98	$2 \times 10^9$	$2.2 \times 10^{-5}$	$2.2 \times 10^{48}$
1	10	1.97	$10^9$	$3.6 \times 10^{-5}$	$1.4 \times 10^{49}$
1	20	1.95	$10^9$	$9.3 \times 10^{-6}$	$3.7 \times 10^{48}$
5	10	1.95	$9 \times 10^8$	$2.7 \times 10^{-7}$	$2.7 \times 10^{48}$
5	20	1.95	$10^9$	$7.5 \times 10^{-8}$	$7.5 \times 10^{47}$
5	40	1.97	$2 \times 10^9$	$2.0 \times 10^{-8}$	$2.0 \times 10^{47}$
5	80	1.97	$2 \times 10^9$	$5.9 \times 10^{-9}$	$5.9 \times 10^{46}$

radio-IR photons emitted by primary electrons in the kpc-scale jet and CMB as well as the AGN photons. The latter photons are important if  $R = 5$  kpc but become less important if  $R$  is smaller when  $f_A = 1$ . The required proton power exceeds the Eddington limit by a few orders of magnitude. However, if the kpc-scale jet receives enhanced beamed radiation from the AGN core, i.e., if 3C 273 is a slightly misaligned blazar, our models do not need the super Eddington power for protons.

### 3.2. PKS 1136–135

Another kpc-scale jet bright in X-rays is PKS 1136–135. The observed spectra of PKS 1136–135 are shown in Figures 8 and 9 for knots A and B, respectively. The data are taken from [Cara et al. \(2013\)](#), [Sambruna et al. \(2006\)](#), and [Uchiyama et al.](#)

(2007). The *Fermi* upper limits from Breiding et al. (2017) are shown by diamonds. The AGN core has visual and NIR luminosities of  $1.1 \times 10^{46} \text{ erg s}^{-1}$  and  $2.2 \times 10^{45} \text{ erg s}^{-1}$ , respectively (Uchiyama et al. 2007). The AGN spectrum is given in Figure 10, which is used to calculate the electron production rate in hadronic processes. We assume  $d_{\text{knot}} = 50 \text{ kpc}$  and  $75 \text{ kpc}$  for knots A and B, respectively. The contribution of soft photons from various sources is shown in Figure 11 for  $f_A = 1$ . In knot A, CMB photons dominate in  $\nu \sim 8 \times 10^{10}$ - $7 \times 10^{11} \text{ Hz}$  and AGN photons dominate otherwise. In knot B, CMB photons dominate in  $\nu \sim 5 \times 10^{10}$ - $10^{12} \text{ Hz}$  and AGN photons dominate otherwise. The parameters for primary electrons are given in Table 1. For simplicity we fix  $R = 5 \text{ kpc}$  in all models. First, we describe knot A. When  $B = 0.1 \text{ mG}$ , we did not find a value of  $\alpha_p$  to fit the data for  $\gamma_{p,\text{max}} = 10^{10}$ , because the flux at  $\sim 10^{14}$  -  $\sim 10^{15} \text{ Hz}$  becomes too large. When the value of  $\gamma_{p,\text{max}}$  is decreased to  $10^9$ , we find that  $\alpha_p = 2.1$  and  $K_p = 3.1 \times 10^{-3} \text{ cm}^{-3}$  fit the X-ray data, though still the slope at  $\sim 10^{14}$  -  $\sim 10^{15} \text{ Hz}$  is too small compared to the observed data. When  $\alpha_p = 1.9$  is assumed,  $\gamma_{p,\text{max}} = 5 \times 10^8$  and  $K_p = 10^{-4} \text{ cm}^{-3}$  fit the X-ray data. Second, we show the results for knot B. Models with parameter sets ( $\alpha_p = 2.2$ ,  $\gamma_{p,\text{max}} = 10^9$ ,  $K_p = 6.57 \times 10^{-2} \text{ cm}^{-3}$ ) and ( $\alpha_p = 1.9$ ,  $\gamma_{p,\text{max}} = 4 \times 10^8$ ,  $K_p = 3.97 \times 10^{-4} \text{ cm}^{-3}$ ), for  $B = 0.1 \text{ mG}$ , are shown in Figure 9. Since these models are not much different from knot A, we discuss only knot A below.

The observed spectrum of knot A is harder at  $\nu \sim 5 \times 10^{14} \text{ Hz}$  than our model spectra. Cara et al. (2013) fit the data with the electron spectral index 2.0 and the large value of the minimum Lorentz factor of electrons, i.e.,  $\sim 3 \times 10^6$ . Unless some acceleration mechanisms exist, it may be difficult to keep this large value of  $\gamma_{e,\text{min}}$  against rapid radiative cooling. Otherwise, different emission regions might contribute.

For knot A with  $f_A = 1$ , we obtain the proton energy  $U_p \sim 1.5 \times 10^{62} \text{ erg}$  for  $B = 0.1 \text{ mG}$ ,  $\alpha_p = 1.9$ ,  $K_p = 10^{-4} \text{ cm}^{-3}$ , and  $\gamma_{p,\text{max}} = 5 \times 10^8$ . The proton power  $L_p$  is  $\sim 9.6 \times 10^{49} \text{ erg s}^{-1}$ . The black hole mass of PKS 1136–135 is estimated to be  $4.6 \times 10^8 M_\odot$  (Oshlack et al. 2002), so that  $L_{\text{Edd}} \sim 10^{47} \text{ erg s}^{-1}$  and  $L_p \sim 10^3 L_{\text{Edd}}$ . This value is similar to the case for 3C 273 and the beaming effect of AGN core emission on the kpc knots is to be considered to suppress the super Eddington of the proton power. When  $f_A = 40$  for knot A, we obtain  $K_p = 3.7 \times 10^{-7}$  and  $L_p \sim 1.5 \times 10^{47} \text{ erg s}^{-1} \sim L_{\text{Edd}}$ . The emission spectra of knots A and B for  $f_A = 40$  are shown in Figures 8 and 9 by circles.

#### 4. SUMMARY AND DISCUSSION

We examined the possibility to explain the X-rays from kpc-scale jets of 3C 273 and PKS 1136–135 by synchrotron radiation emitted by electrons/positrons produced by Bethe-Heitler process. We explored various conditions such as the size of the emission region, the soft photon injection from the AGN core, the spectral shape of protons, and the proton power.

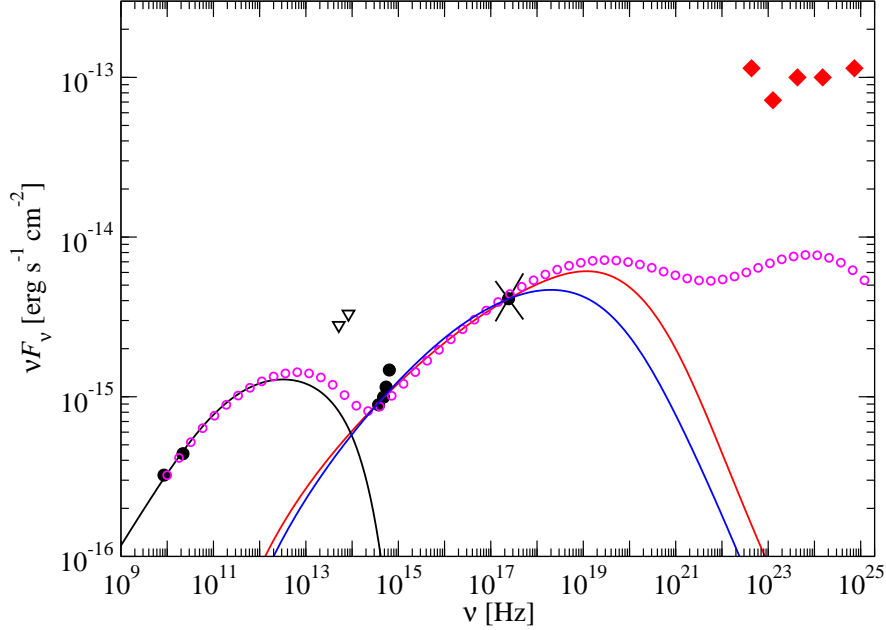


**Figure 8.** The spectral energy distribution of knot A of PKS 1136–135 (filled circles). Triangles and diamonds are upper limits. For the models  $R = 5$  kpc,  $B = 0.1$  mG, and  $d_{\text{knot}} = 50$  kpc are assumed. Solid red line:  $f_A = 1$ ,  $\alpha_p = 2.1$ ,  $\gamma_{p,\text{max}} = 10^9$ , and  $K_p = 3.1 \times 10^{-3} \text{ cm}^{-3}$ . Solid blue line:  $f_A = 1$ ,  $\alpha_p = 1.9$ ,  $\gamma_{p,\text{max}} = 5 \times 10^8$ , and  $K_p = 10^{-4} \text{ cm}^{-3}$ . The emission spectrum for  $f_A = 40$  is shown by open circles, where  $\alpha_p = 1.98$ ,  $\gamma_{p,\text{max}} = 2 \times 10^9$ , and  $K_p = 3.7 \times 10^{-7} \text{ cm}^{-3}$ . This spectrum is the sum of IC scattering by primary electrons and synchrotron radiation by primary electrons and electrons/positrons produced by Bethe-Heitler and photo-pion processes.

Because the efficiency of electron/positron production by Bethe-Heitler process is low, the proton power larger than the Eddington limit is required to explain the X-rays from the knots of 3C 273 and PKS 1136–135 as for PKS 0637–752. Observations show that there indeed exist AGNs with super-Eddington luminosity (e.g., Jin et al. 2017, and references therein). However, our models for 3C 273 and PKS 1136–135 require the proton power much larger than the Eddington limit, e.g.,  $\sim 10^2\text{--}10^4 L_{\text{Edd}}$ . Then we presented a model with a reduced proton power, which assumes that the radiation from the AGN core to the knots is enhanced by the relativistic beaming. Here the axis of the AGN core jet is slightly off the line of sight, so that the observed AGN flux is smaller than the flux received by the knots. If the number flux per unit frequency received by the knots is about 10–40 times larger than that observed by us, the required proton power becomes about the Eddington limit. When this is the case, IC scattering by primary electrons also increases the flux in GeV band. Since the sum of this contribution and emission by electrons/positrons from photo-pion processes should be lower than the *Fermi* upper limits, the upper bound of the enhancement factor  $f_A$  is less than  $\sim 80$  for 3C 273. For PKS 1136–135,  $f_A$  can be larger because the constraint by the *Fermi* limit is weaker. According to Sambruna et al. (2001) the brightness distribution between X-rays and radio are different in 3C 273 (see also Marchenko et al. 2017). While radio emission is brighter at the outer edge of the



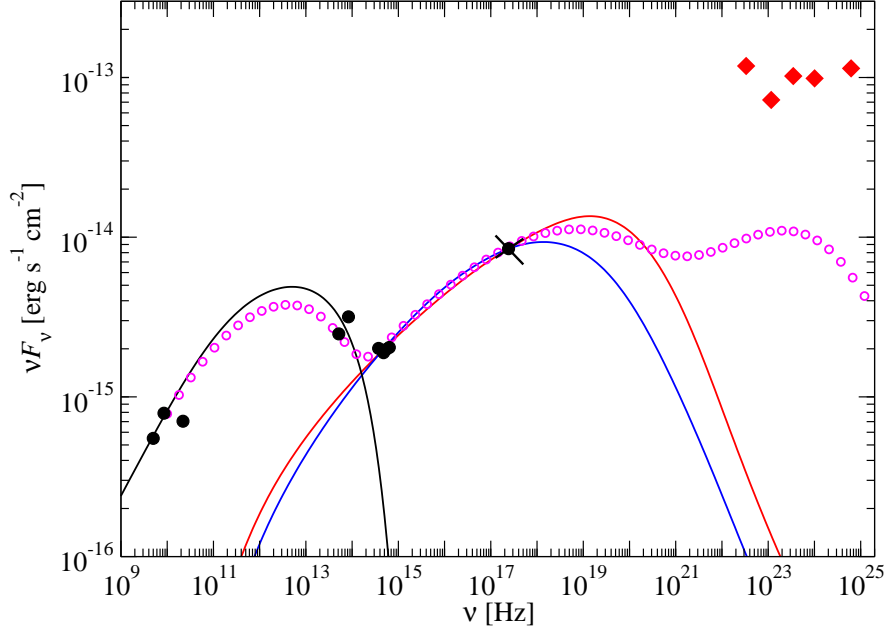


**Figure 9.** The spectral energy distribution of knot B of PKS 1136–135 (filled circles). The red diamonds are the *Fermi* upper limits. For the models  $R = 5$  kpc,  $B = 0.1$  mG, and  $d_{\text{knot}} = 75$  kpc are assumed. Red solid line:  $f_A = 1$ ,  $\alpha_p = 2.2$ ,  $\gamma_{p,\text{max}} = 10^9$ , and  $K_p = 6.57 \times 10^{-2} \text{ cm}^{-3}$ . Blue solid line:  $f_A = 1$ ,  $\alpha_p = 1.9$ ,  $\gamma_{p,\text{max}} = 4 \times 10^8$ , and  $K_p = 3.97 \times 10^{-4} \text{ cm}^{-3}$ . The emission spectrum for  $f_A = 40$  is shown by open circles, where  $\alpha_p = 1.98$ ,  $\gamma_{p,\text{max}} = 10^9$ , and  $K_p = 2.1 \times 10^{-6} \text{ cm}^{-3}$ . This spectrum is the sum of IC scattering by primary electrons and synchrotron radiation by primary electrons and electrons/positrons produced by Bethe-Heitler and photo-pion processes.

jet, X-rays are stronger at inner portion. This may imply the photons from the AGN core play a role in X-ray emission in the large scale jet by Bethe-Heitler process.

As for the size of the emission region, in the hadronic model with enhanced AGN photons, a smaller size model needs more proton power than a larger one for a given value of  $f_A$ . For example, the value of  $L_p$  of a knot with  $R = 0.5$  kpc of 3C 273 is larger by a factor  $\sim 10$  than that with  $R = 5$  kpc.

We briefly comment on the effects of AGN photons on PKS0637–752, which was not covered in our previous paper. As for PKS 0637–752, [Edwards, et al. \(2006\)](#) reported superluminal motion of the pc-scale jet. Core optical luminosity is about three orders of magnitude higher than that of the knot. The projected distance to the knot from the core is about 70 kpc so that the radiation from the core can be ignored if the beaming effect is neglected. Only if the core is not aligned with the line of sight and the kpc-scale jet is aligned with beamed radiation, the core emission may be effective. When we adopt a small viewing angle, the distance of the knot becomes as large as Mpc, which is unlikely. The spectral energy distribution of the core seems to be a little different from a typical blazar; the luminosity of the high energy component is mild ([Meyer et al. 2017](#)). Thus the possibility of a slightly off

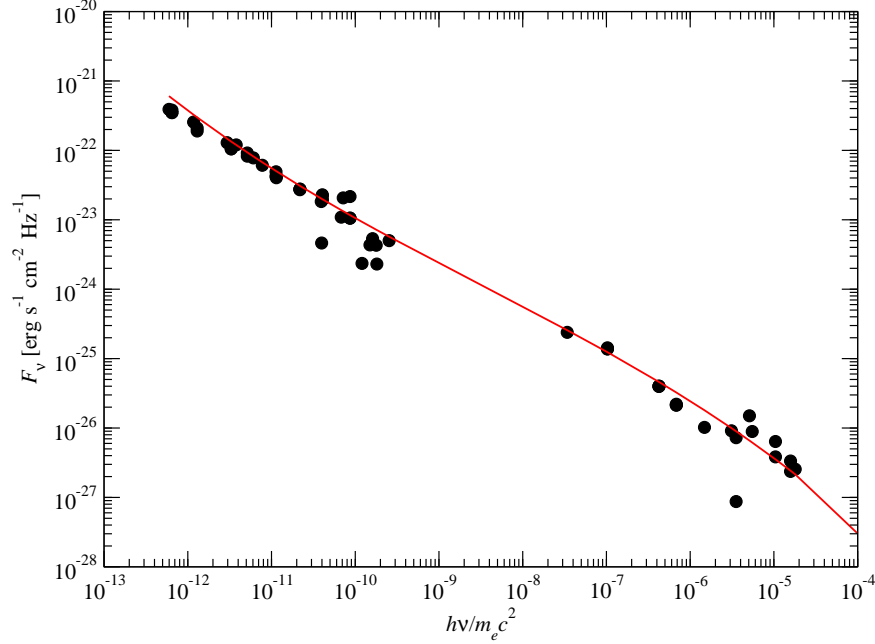


**Figure 10.** The radiation spectrum of PKS 1136–135. Filled circles are the data from NED. The red line is a polynomial fit of the  $\log \nu$ - $\log F_\nu$  representation and used in calculations of electron/positron production.

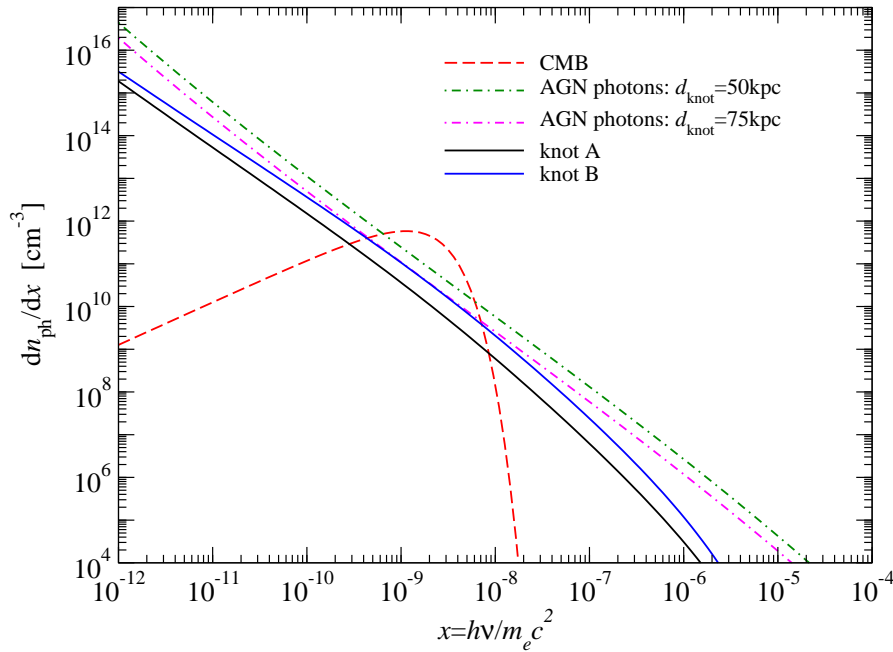


**Figure 11.** The target photon spectra for proton-photon collisions for PKS 1136–135. The synchrotron radiation by primary electrons in knot A and knot B are shown by the black and blue solid lines, respectively. CMB photons are shown by the red dashed line. The green and magenta dot-dashed lines are the AGN photons with  $f_A = 1$  for  $d_{\text{knot}} = 50$  and 75 kpc, respectively.

beamed jet cannot be neglected. If this is the case, the kpc-scale jet may see an order of magnitude larger beamed radiation.

The cascade of  $\gamma$ -rays produced by  $\pi^0$  decay is not included in this work. The optical depth of the electron-positron pair production in photon-photon collisions is  $\tau_{\gamma\gamma} \sim \sigma_T n_{\text{soft}} R$  for the threshold photon energies, where  $\sigma_T$  is the Thomson cross section and  $n_{\text{soft}}$  is the target soft photon number density. For a knot of 3C 273 with  $R = 5$  kpc,  $B = 0.1$  mG, and  $f_A = 40$ , we find  $\tau_{\gamma\gamma} \gtrsim 1$  for  $\nu \gtrsim 3 \times 10^{24}$  Hz or  $h\nu \gtrsim 12$  GeV. The produced  $\gamma$ -ray spectrum has a peak at  $\nu \sim 10^{29}$  Hz and its production rate is similar to that of positrons. Then electron-positron pairs produced by  $\gamma$ -rays emit synchrotron radiation with a spectrum similar to that of positrons via photo-pion processes. Thus the  $\gamma$ -ray flux may be as twice as that of positron synchrotron radiation.

In this work we did not consider the relativistic bulk motion of the knots towards us. When the knots have the beaming factor larger than unity, the soft photon density by primary electrons is reduced to account for the observed radio-IR spectrum. This results in the lower electron production rate by Bethe-Heitler process. Photons from the AGN core received by the knots also decrease, while CMB radiation is enhanced in the knot frame and IC/CMB process becomes effective.

Our model does not satisfy the equipartition condition, i.e., the energy density of protons is much larger than that of magnetic fields. Furthermore, we assumed the acceleration of protons is more efficient than that of the primary electrons. That is, the proton power is larger than the electron power, and the maximum Lorentz factor of protons is also larger than that of the primary electrons. However, these issues, equipartition and acceleration, are beyond the scope of this paper.

This research has made use of the NASA/IPAC Extragalactic Database (NED) which is operated by the Jet Propulsion Laboratory, California Institute of Technology, under contract with the National Aeronautics and Space Administration.

## REFERENCES

- Aharonian, F. A. 2002, MNRAS, 332, 215  
 Bhattacharyya, W., & Gupta, N. 2016, ApJ, 817, 11  
 Breiding, P., Meyer, E. T., Georganopoulos, M., et al. 2017, ApJ, 849, 95  
 Cara, M., Perlman, E. S., Uchiyama, Y., et al. 2013, ApJ, 773, 186  
 Celotti, A., Ghisellini, G., & Chiaberge, M. 2001, MNRAS, 321, L1  
 Chartas, G., Worrall, D. M., Birkinshaw, M., et al. 2000, ApJ, 542, 655  
 Edwards, P. G., Piner, B. G., Tingay, S. J., et al. 2006, PASJ, 58, 233  
 Espaillat, C., Bregman, J., Hughes, P., & Lloyd-Davies, E. 2008, ApJ, 679, 182  
 Fan, J. H., Peng, Q. S., Tao, J., Qian, B. C., & Shen, Z. Q. 2009, ApJ, 138, 1428  
 Ghisellini, G., Righi, C., Costamante, L., & Tavecchio, F. 2017, MNRAS, 469, 255  
 Jester, S., Röser, H.-J., Meisenheimer, K., & Perley, R. 2005, A&A, 431, 477  
 Jin, C., Done, C., Ward, M., & Gardner, M. 2017, MNRAS, 471, 706  
 Kataoka, J., & Stawarz, L. 2005, ApJ, 622, 797  
 Kelner, S. R., & Aharonian, F. A. 2008, PhRvD, 78, 034013

- Kusunose, M., & Takahara, F. 2017, *ApJ*, 835, 20
- Liu, W.-P., Chen, Y. J., & Wang, C.-C. 2015, *ApJ*, 806, 188
- Liu, R. -Y., Rieger, F. M., & Aharonian, F. A. 2017, *ApJ*, 842, 39
- Marchenko, V., Harris, D. E., Ostrowski, M., Stawarz, L., & Bohdan, A. 2017, *ApJ*, 844, 11
- Meyer, E. T., & Georganopoulos, M. 2014, *ApJL*, 780, L27
- Meyer, E. T., Georganopoulos, M., Sparks, W. B., et al. 2015, *ApJ*, 805, 154
- Meyer, E. T., Breiding, P., Georganopoulos, M., et al. 2017, *ApJL*, 835, L35
- Oshlack, A. Y. K. N., Webster, R. L., & Whiting, M. T. 2002, *ApJ*, 576, 81
- Paltani, S., & Türler, M. 2005, *A&A*, 435, 811
- Sambruna, R. M., Urry, C. M., Tavecchio, F., et al. 2001, *ApJL*, 549, L161
- Sambruna, R. M., Gliozzi, M., Donato, D., et al. 2006, *ApJ*, 641, 717
- Schwartz, D. A., Marshall, H. L., Lovell, J. E., et al. 2000, *ApJL*, 540, L69
- Tavecchio, F., Maraschi, L., Sambruna, R. M., & Urry, C. M. 2000, *ApJL*, 544, L23
- Tavecchio, F., Maraschi, L., Sambruna, R. M., Gliozzi, M., Cheung, C. C., Wardle, J. F. C., & Urry, C. M. 2006, *ApJ*, 641, 732
- Uchiyama, Y., Urry, C. M., Cheung, C. C., et al. 2006, *ApJ*, 648, 910
- Uchiyama, Y., Urry, C. M., Coppi, P., et al. 2007, *ApJ*, 661, 719